Liquid Crystals
Publication details, including instructions for authors and subscription information:
http://www.informaworld.com/smpp/title~content=t713926090

Morphological phase behaviour of a homologous series of thermotropic cubic mesogens under pressure

Yoji Maeda[a]; Hiroyuki Mori[b]; Shoichi Kutsumizu[b]
[a] Department of Life Science and Sustainable Chemistry, Faculty of Engineering, Tokyo Polytechnic University, 1583 Iiyama, Atsugi, Kanagawa, Japan [b] Department of Chemistry, Faculty of Engineering, Gifu University, 1-1, Yanagido, Gifu, Japan

Online publication date: 23 April 2010

To cite this Article Maeda, Yoji , Mori, Hiroyuki and Kutsumizu, Shoichi(2010) 'Morphological phase behaviour of a homologous series of thermotropic cubic mesogens under pressure', Liquid Crystals, 37: 4, 463 — 473
To link to this Article: DOI: 10.1080/02678291003653658
URL: http://dx.doi.org/10.1080/02678291003653658

Liquid Crystals,
Vol. 37, No. 4, April 2010, 463–473

Taylor & Francis
Taylor & Francis Group

Morphological phase behaviour of a homologous series of thermotropic cubic mesogens under pressure

Yoji Maeda[a]*, Hiroyuki Mori[b] and Shoichi Kutsumizu[b]

[a]*Department of Life Science and Sustainable Chemistry, Faculty of Engineering, Tokyo Polytechnic University, 1583 Iiyama, Atsugi, Kanagawa 243-0297, Japan;* [b]*Department of Chemistry, Faculty of Engineering, Gifu University, 1-1 Yanagido, Gifu 501-1193, Japan*

(Received 30 December 2009; final version received 26 January 2010)

The phase behaviour of a homologous series of thermotropic cubic mesogens of 1,2-bis(4'-*n*-alkoxybenzoyl)hydrazines (BABH-*n,* where *n* is the number of carbon atoms in both terminal alkoxy chains, ranging from $n = 11$ to $n = 18$) was studied under hydrostatic pressure using a polarising optical microscope (POM) equipped with a high-pressure optical cell. Pressure-temperature phase diagrams were constructed for all the samples. All of the samples showed the crystal (Cr)–cubic (Cub)–isotropic liquid (I) phase sequence under atmospheric and lower pressures, but the Cub phase was replaced completely by a high-pressure smectic C (SmC) phase; SmC(hp), under higher pressures. There is an intermediate-pressure region as a boundary in which the Cr–SmC(hp)–Cub–I phase sequence was recognised. The SmC(hp)–Cub transition lines showed positive slopes with pressure and shifted to higher pressures with increasing alkoxy chain length in BABH-*n*. What should noted here is the inversion of the Cub and SmC phases in the phase sequence, in comparison to those (Cr–Cub–SmC–I) for BABH-8 and -10. In BABH-14, -16 and -18, a solid state with a featureless texture and stronger intensities of transmitted POM light appeared just below the SmC(hp) phase on cooling under intermediate and high pressures. This phenomenon is not due to the formation of a monotropic Cub phase but is an induction period for spherulitic crystallisation from the SmC(hp) phase.

Keywords: thermotropic cubic mesogen; high-pressure smectic C phase; pressure-temperature phase diagram; inversed phase sequence between cubic and smectic C phases

1. Introduction

1,2-bis(4'-*n*-alkoxybenzoyl)hydrazine (BABH-*n*, where *n* indicates the number of carbon atoms in the alkoxy group) is known as one of classical thermotropic cubic mesogens. BABH-*n* molecules are composed of a rigid aromatic core at the centre and flexible aliphatic chains at the ends of the molecules. The chemical structure of BABH-*n* is:

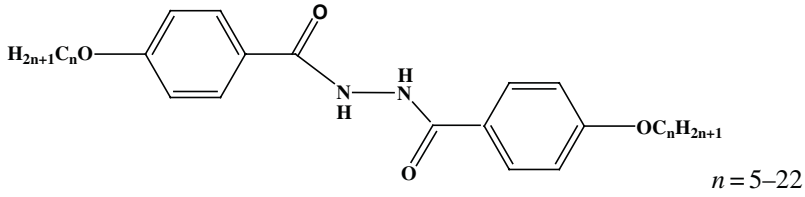

As reported by Schubert *et al.* [1] and Demus *et al.* [2], BABH-8, -9 and -10 having octyloxy, nonyloxy and decyloxy groups, respectively, exhibit an unusual phase sequence of crystal (Cr)–cubic (Cub)–smectic C (SmC)–isotropic liquid (I), in contrast to the usual phase sequence of Cr–SmC–Cub–I of many cubic mesogens showing Cub and SmC phases [3–10]. BABH-8 has the *Ia3d* cubic structure, which consists of two pairs of 3×3 interpenetrating networks [11–13]. Two of the authors extended the previous work and revealed the phase behaviour from $n = 5$ to $n = 22$; the alkoxy chain members other than $n = 8 \sim 10$ show the Cr–Cub–I phase sequence under atmospheric pressure [14–16]. The BABH-*n* system exhibits two types of Cub phases, *Ia3d* and *Im3m*, i.e. BABH-6∼BABH-12 and BABH-17∼BABH-22 take the *Ia3d* type, and BABH-14 exhibits the *Im3m* type. BABH-13, -15 and -16 have both types.

The authors reported the pressure–temperature (*P*–*T*) phase diagrams of BABH-8 [17] and -10 [18], and, although partly incomplete, the phase diagrams of BABH-11 and -12 [19] using mainly a high-pressure

*Corresponding author. Email: ymaeda@nano.t-kougei.ac.jp

ISSN 0267-8292 print/ISSN 1366-5855 online

DOI: 10.1080/02678291003653658
http://www.informaworld.com

differential thermal analyser. In BABH-8 and -10, the Cr–*Ia3d*-Cub and SmC–I transition lines show typically positive slopes (dT/dP) with pressure, while the *Ia3d*-Cub–SmC transition line exhibits a negative slope. Accordingly, a triple point appears at a relatively low pressure in which the Cr, *Ia3d*-Cub and SmC phases meet. Their triple points are reported to be about 32 and 11 MPa for BABH-8 and -10, respectively, indicating the upper limit of pressure for the formation of the Cub phase. On the other hand, BABH-11 and -12 show the Cr–*Ia3d*-Cub–I phase sequence under atmospheric and lower pressures below 10–11 MPa and 16–17 MPa, respectively, beyond which the Cub phase is replaced completely by a high-pressure SmC phase (SmC(hp)). In this case the SmC phase is a high-pressure phase because the phase goes back to the Cub phase when pressure is released to atmospheric pressure. Unfortunately the Cub–SmC(hp) transition lines are not determined yet in the phase diagrams of BABH-11 and -12, only the maximum pressure for the Cub phase has been deduced [19].

We reported recently the inversion of the phase sequence between the Cub and SmC phases in the homologous BABH-8 and -14 compounds, in which the SmC(hp)–Cub transition for BABH-14 appears in the intermediate-pressure region [20]. This finding urged us to investigate extensively the phase behaviour of other BABH-*n* compounds under hydrostatic pressure.

2. Experimental

The phase transition behaviour under pressure for BABH-11, -12, -16 and -18 was studied by using a polarising optical microscope (POM). The phase behaviour of BABH-8, -10 and -14 have already been reported [18, 20] and the results are included herein. All of the samples used in this study were prepared as described elsewhere [14–16]. The morphological observation was performed using an Olympus BX51 POM equipped with a high-pressure optical system [21]. The high-pressure system uses a silicone oil with a low-viscosity (10 centistokes) (TSF 451-10, Toshiba Silicone Co., Tokyo, Japan) as the pressure medium and the system can apply hydrostatic pressure up to 200 MPa. The high-pressure hot stage has a pair of sapphire optical windows at the top and bottom centres of the steel cell. The Cub and I phases at atmospheric pressure are observed usually as a black field of view under crossed polarisers, but the phases at hydrostatic pressures can be seen brightly under parallel polarisers. Accordingly the textures of the Cub and I phases could be observed distinctively under pressures. Intensity (I) of the transmitted POM light was measured using a Mettler FP-90 photomonitor connected with the FP90 central processor. The I–temperature (T) curve is useful in determining a transition point because it enables a discontinuous change of intensity to be exhibited at each phase transition. The texture observation and intensity measurement of transmitted POM light were performed simultaneously both on heating and cooling at a scanning rate of about 1–2°C min^{-1} under pressures up to 120 MPa.

3. Results

3.1 BABH-8 and BABH-10

BABH-8 and -10 showed the unusual phase sequence of Cr–*Ia3d*-Cub–SmC–I under atmospheric pressure compared with the usual phase sequence of Cr–SmC–Cub–I for many other cubic mesogens [3–10]. Figure 1 shows the P–T phase diagrams of BABH-8 and -10 constructed on heating, which were reported previously [17, 18, 20]. Both compounds show the *Ia3d*-Cub–SmC transition lines of negative slopes ($dT/dP < 0$) with pressure in their diagrams and thus, the triple points appear at the relatively low pressures of about 24 and 10 MPa for BABH-8 and -10, respectively, indicating the upper limit of pressure for the formation of the Cub phase. The triple points determined by the POM method were more accurate than those measured by high-pressure differential thermal analysis (DTA) at high scanning rates such as 5–10°C min^{-1}.

3.2 BABH-11 and BABH-12

BABH-11 and -12 are known to take the *Ia3d*-type cubic structure [14–16]. Applying pressure on the Cub phases of BABH-11 and -12 induces the formation of the SmC(hp) phase [19]. In order to complete the P–T phase diagrams, the phase behaviours of BABH-11 and -12 were reinvestigated, especially in the boundary regions.

Figure 2 shows the I–T curves of BABH-11 at three pressures of 1, 3 and 12 MPa, respectively. The I–T curve on heating at 1 MPa shows three steps from the room-temperature crystal (Cr_2) to the isotropic liquid (I). By simultaneous texture observation, the first and second steps were due to the crystal (Cr_2)–crystal (Cr_1) and the successive Cr_1–*Ia3d*-Cub transitions, respectively. The reversible phase transition at 1 MPa was recognised as Cr_2–Cr_1–*Ia3d*-Cub–I, in which the phase sequence is the same as one observed at atmospheric pressure. Spherulitic crystallisation occurred smoothly from the Cub phase in the low-pressure region. At 3 MPa, the I–T curve on heating showed

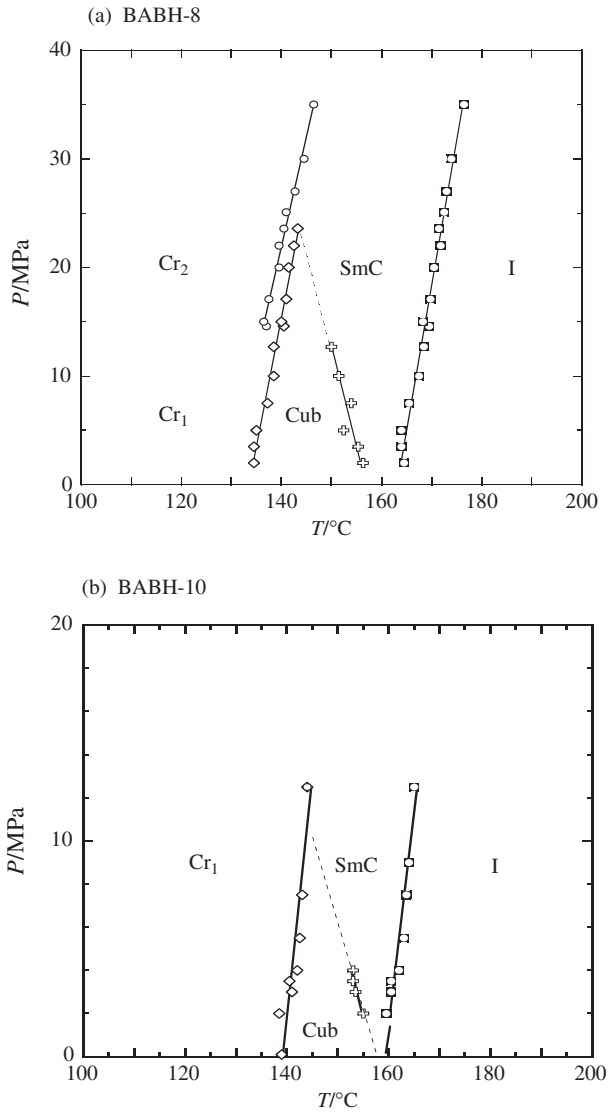

Figure 1. Pressure–temperature phase diagrams of (a) BABH-8 and (b) BABH-10 constructed on heating (reproduced from [17, 18, 20]).

the same three-step pattern as that observed at 1 MPa. The subsequent cooling, however, exhibited a strange behaviour as shown in Figure 2(b): the intensity decreased first at the isotropisation point and then was held for a while on cooling, but the intensity increased again to the level of the I phase. The subsequent heating showed a high level of intensity for the isotropic liquid in the whole temperature region. Figure 3 shows the change in texture of the sample on cooling at 3 MPa. The texture (Figure 3(b)) at 157°C shows the growing spheres of the SmC phase born from the isotropic liquid (Figure 3(a)) and the spheres were coalesced to the continuous texture (Figure 3(c)) of the SmC phase at 155°C, which indicates the growth of a thread-like texture. Then, the thread-like texture changed suddenly to the

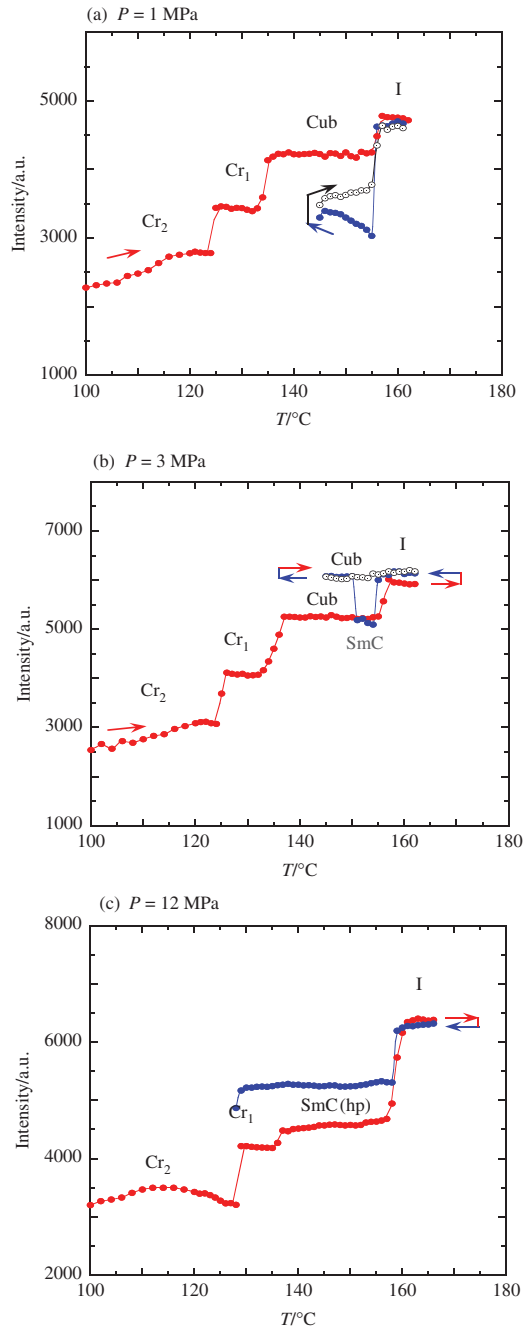

Figure 2. Intensity–temperature curves of BABH-11 at (a) 1 MPa, (b) 3 MPa and (c) 12 MPa.

featureless one (Figure 3(d)) of an optically isotrophic phase at 152°C. The textural change in Figure 3 indicates the formation and growth of the SmC phase, followed by the transformation to the *Ia3d*-type Cub phase. At that time the SmC–*Ia3d*-Cub transition points were scattered remarkably, depending upon the cooling condition and pressure. The SmC phase appeared only on cooling under pressures between 3 and 7 MPa. On subsequent heating, the Cub phase was transformed directly to the isotropic liquid.

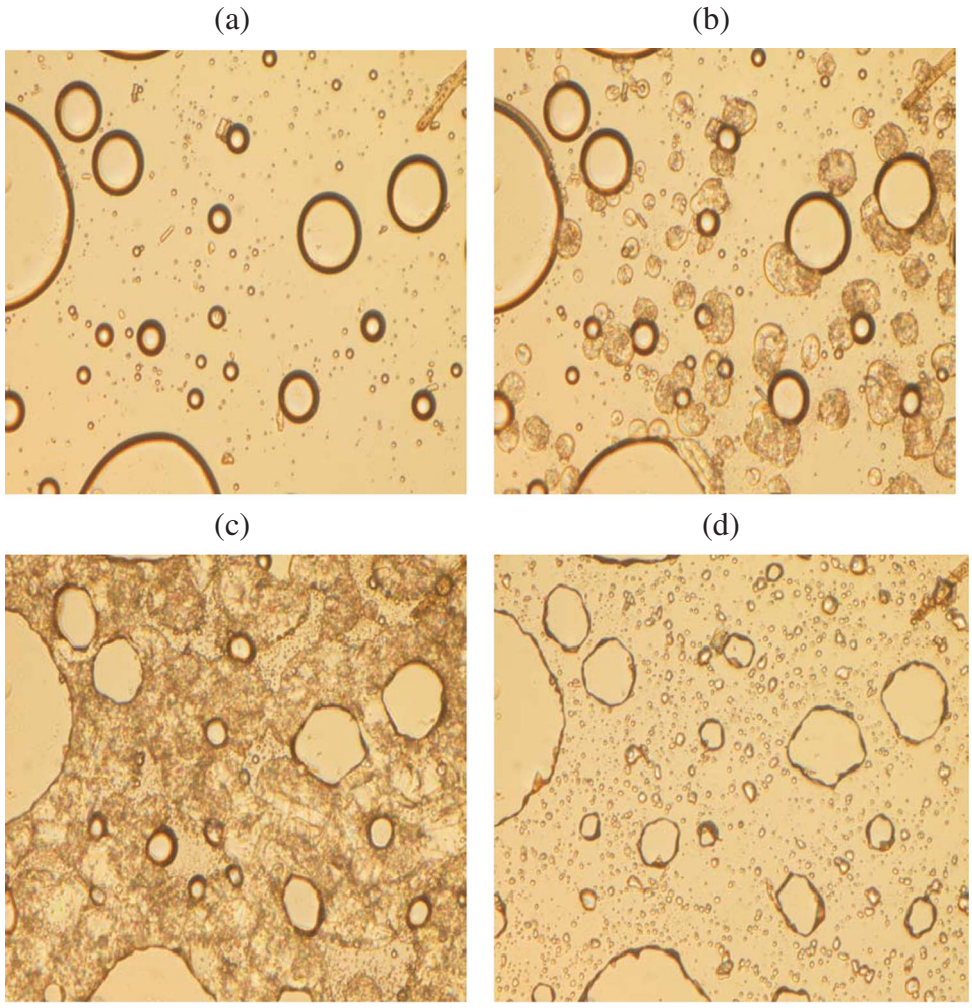

Figure 3. Polarising optical microscopy textures of BABH-11 on cooling at 3 MPa: (a) the isotropic liquid at 159°C; (b) the isotropic liquid-smectic C phase transition at 157°C; (c) the smectic C phase at 155°C; (d) the cubic phase at 152°C (colour version online).

Accordingly the phase sequence at 3 MPa was recognised as I–SmC–Cub–Cr_1 on cooling, but Cr_1–Cub–I on heating, respectively. Next the SmC phase just formed was annealed at temperatures below the isotropisation point to estimate phase stability. The SmC phase was formed rapidly from the isotropic liquid, but the phase was transformed into the Cub phase after annealing for 10 min. Since the SmC phase is not stable, it can be understood as an unstable phase.

Furthermore the phase behaviour observed at intermediate pressures between 7 and 10 MPa led to confusion. Another SmC phase, i.e., SmC(hp), began to appear between the Cr and Cub phases, and the Cr–SmC(hp)–*Ia3d*-Cub–I phase transition was observed on heating. However, the SmC(hp) phase was difficult to see on cooling from the isotropic liquid. Figure 4 shows the change in texture of BABH-11 by cooling at 9.5 MPa and then annealing at 140°C. In Figure 4(a) a sand-like texture of the Cub phase is exhibited at 157°C, which was formed from the isotropic liquid. On cooling at 140°C, a small region with a fine thread-like texture appeared in the Cub phase, near the bubble on the right side in Figure 4(b). The region with a fine thread-like texture enlarged slightly with annealing, indicating the gradual growth of the SmC(hp) phase. Since the growth rate of the SmC(hp) phase was very small, the region was still small even after annealing for 90 min, as shown in Figure 4(c). It was suggested that the completion of the Cub–>SmC(hp) transition took more than about 5–6 hours. On the other hand, the reversible transformation between the cubic and SmC(hp) phases was confirmed by the isothermal pressurising experiments at 140 and 150°C. Therefore, it was concluded that the Cr–SmC(hp)–Cub–I phase transition is substantially reversible in the intermediate-pressure region. Here the two SmC phases for BABH-11 (i.e. unstable SmC and stable SmC(hp) phases), were recognised under low

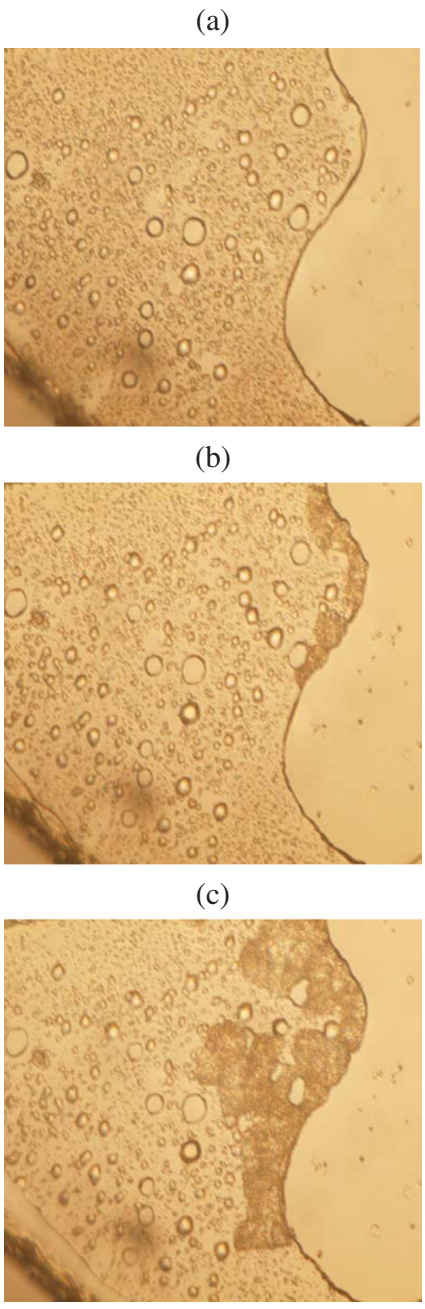

Figure 4. Change in texture of the cubic phase of BABH-11 by cooling at 9.5 MPa and then annealing at 140°C: (a) the cubic phase at 157°C; (b) the coexistant cubic and high-pressure smectic C phases at 140°C; (c) the coexistant cubic and high-pressure smectic C phases annealed at 140°C for 90 min (colour version online).

and intermediate pressures, respectively. The unstable SmC phase is related to the SmC phase for BABH-8 and -10 because this phase exists at the high temperature side of the cubic phase [17, 18]. On the other hand, the SmC(hp) phase appears at the low temperature side of the Cub phase in the intermediate-pressure region.

Returning to Figure 2, the *I–T* curve in Figure 2(c) shows a three-step pattern of Cr–SmC(hp)–I phase sequence under high pressures. The SmC(hp) phase appears reversibly as only one mesophase between the Cr_1 form and the I phase. The SmC(hp) phase was seen commonly in BABH-12, -14, -16 and -18 and is described below.

Figure 5 shows the *P–T* phase diagrams of BABH-11 constructed on heating and cooling. The phase behaviour is divided into three pressure regions, i.e., the low-pressure region below 7 MPa, the intermediate-pressure region, and the high-pressure region above about 10 MPa. In Figure 5(a), two triple points can be seen. One is 7 MPa and 138°C, at which the Cr_1, SmC(hp) and *Ia3d*-type Cub phases meet. The other is 10 MPa and 165°C, at which the SmC(hp), *Ia3d*-type Cub and I phases meet. These indicate the lower and higher limits of pressure for the formation of the SmC(hp) and Cub phases, respectively. The SmC(hp)–*Ia3d*-Cub transition line connecting the two triple points has a positive and steep slope with pressure. The phase sequences of BABH-11 in the low-, intermediate- and high-pressure regions were recognised as Cr–*Ia3d*-Cub–I, Cr–SmC(hp)–*Ia3d*-Cub–I, and Cr–SmC(hp)–I, respectively.

The high-pressure DTA study showed that BABH-12 has almost the same behaviour as that of BABH-11 [19]. This conclusion has not been substantially changed by the present refinement, but analysis of the *I–T* curves allowed us to divide clearly the behaviour into three pressure regions, i.e., the low-pressure region below 5 MPa, the intermediate-pressure region, and the high-pressure region above 10 MPa. The only difference in BABH-12 is that there was no recognition of the unstable SmC phase as observed for BABH-11. BABH-12 also showed a kinetically asymmetrical behaviour of the SmC(hp)–*Ia3d*-Cub transition in the intermediate-pressure region: the SmC(hp) to *Ia3d*-Cub transformation was observed usually on heating, but the reverse (*Ia3d*-Cub to SmC(hp)) was too slow to be observed. The cooling process induced the supercooling of the *Ia3d*-Cub phase until crystallisation occurred. The SmC(hp) phase could be confirmed by annealing on the way to cooling.

On the other hand, the SmC(hp) phase in the high-pressure region was formed rapidly from the isotropic liquid. Many small spheres of the SmC(hp) phase were formed sporadically in the isotropic liquid at 23 MPa and then the spheres were coalesced rapidly to form the continuous texture. Then the SmC(hp) phase transformed into the crystalline phase on further cooling. The *P–T* phase diagram of BABH-12 constructed on heating is shown in Figure 6. Two triple points can be seen. One is 5 MPa and 131°C, at which the Cr,

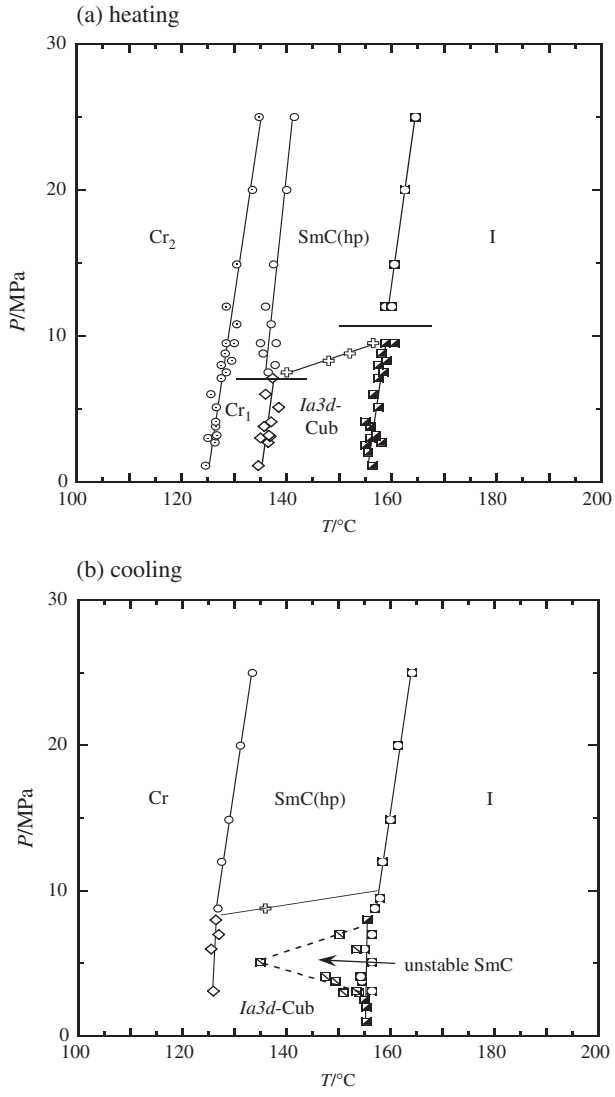

Figure 5. Pressure–temperature phase diagrams of BABH-11 constructed on (a) heating and (b) cooling.

SmC(hp) and *Ia3d*-Cub phases meet. The other is 10 MPa and 160°C, at which the SmC(hp), *Ia3d*-Cub and I phases meet. The SmC(hp)–*Ia3d*-Cub transition line has a positive and steep slope with pressure, as seen in the case of BABH-11.

3.3 BABH-14

BABH-14 takes the *Im3m*-type cubic structure under atmospheric pressure [16]. The phase behaviour of BABH-14 under pressure was reported recently [20]. The *P*–*T* phase diagrams constructed on heating and cooling are reproduced in Figure 7; the phase behaviour is divided into three pressure regions of the low-, intermediate- and high-pressure regions. In the *P*–*T* phase diagram on heating, one can see two triple points. One is 15 MPa and 133°C, at which the Cr,

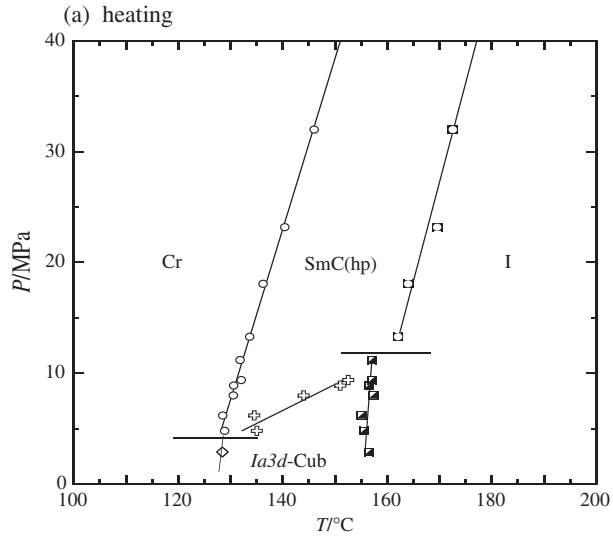

Figure 6. Pressure–temperature phase diagram of BABH-12 constructed on heating.

SmC(hp) and *Im3m*-Cub phases meet. The other is 36 MPa and 163°C, at which the SmC(hp), *Im3m*-Cub and I phases meet. The two triple points indicate the lower and higher limits of pressure for the formation of the SmC(hp) and Cub phases, respectively. The SmC(hp)–Cub transition line has a positive and gentle slope with pressure.

The I–Cub–SmC(hp) transition occured on cooling in the intermediate-pressure region. On further cooling, a strange solid state often appeared below the SmC(hp) phase, in which the intensity of transmitted light increased to high levels comparable to those of the Cub and I phases [20]. Then the crystalline textures were grown slowly at lower temperatures. At first this phenomenon was thought to be a phase transition between the SmC(hp) and monotropic Cub phases; however, this phase was not a Cub phase but a solid state before spherulitic crystallisation. An X-ray diffraction analysis did not show the formation of a Cub phase, but often exhibited spot-like patterns similar to those of single crystals. This might be the appearance of an induction period before spherulitic crystallisation from the SmC(hp) phase in the intermediate- and high-pressure regions. Such a kinetic phenomenon was commonly seen for the homologous BABH-16 and -18 with longer alkoxy chains. An X-ray structural analysis on phase behaviour for the Cub phases will be presented shortly.

3.4 BABH-16

BABH-16 has two types of cubic structures, i.e., *Im3m* and *Ia3d*, in the lower and higher temperature regions, respectively, at atmospheric pressure [16]. Unfortunately

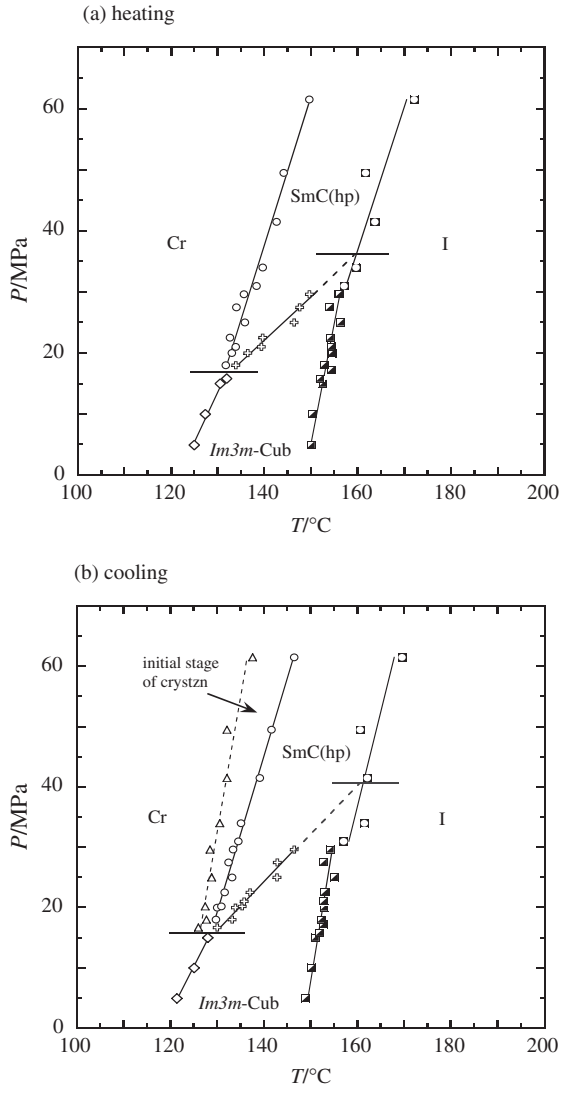

Figure 7. Pressure–temperature phase diagrams of BABH-14 constructed on (a) heating and (b) cooling.

the Cub phases cannot be discriminated by POM experiments. So we temporally handled the phase behaviour as one Cub phase between the Cr and I phases. Figure 8 shows three *I–T* curves of BABH-16 at 10, 42 and 69 MPa. Similarly the phase behaviour is divided into three pressure regions, the low-pressure region below 28 MPa, the intermediate-pressure region, and the high-pressure region above about 47 MPa. The *I–T* curves shown in Figure 8 are representatives of phase behaviour in each pressure region. The *I–T* curve in Figure 8(a) shows simply the Cr–Cub–I phase sequence in the low-pressure region. The *I–T* curve in Figure 8(b) exhibits the Cr–SmC(hp)–Cub–I phase sequence in the intermediate-pressure region on heating, but the I–Cub–SmC(hp)–*solid*–Cr phase sequence was recognised on cooling. Figure 9 shows the corresponding

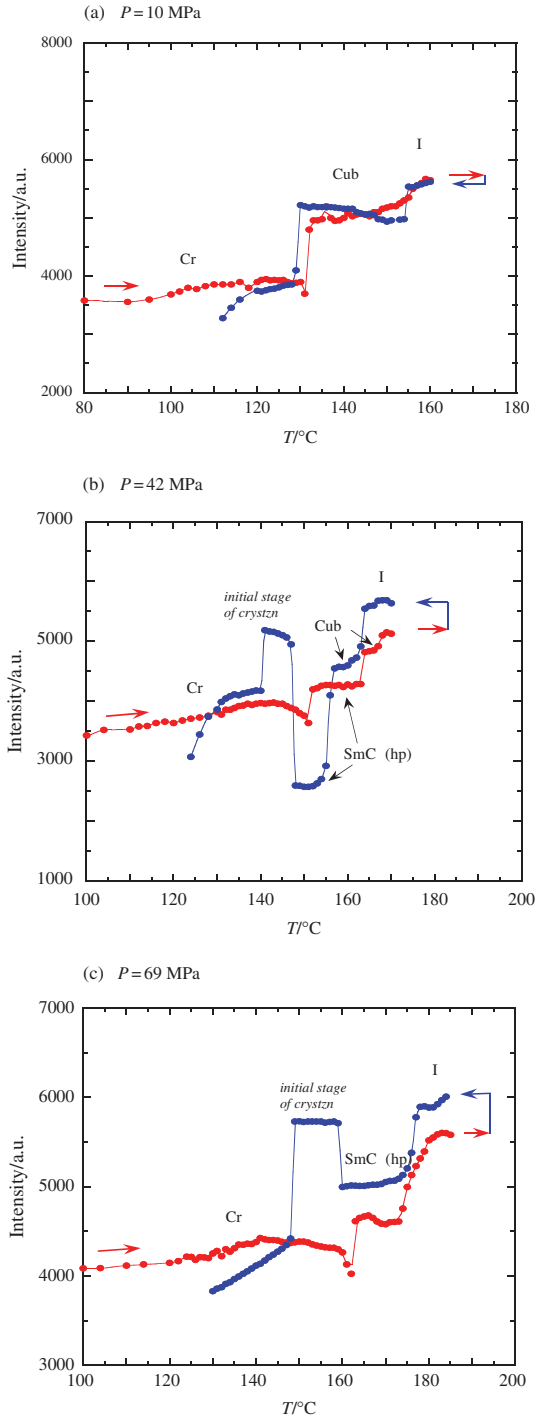

Figure 8. Intensity–temperature curves of BABH-16 at (a) 10 MPa, (b) 42 MPa and (c) 69 MPa.

textural change recorded on cooling at 42 MPa. The isotropic liquid (168°C) (Figure 9(a)) was clear and uniform and then changed to the sand-like texture of the Cub phase (163°C) (Figure 9(b)). Then, dark brown lumps with a very fine thread-like texture for the SmC(hp) phase (155°C) (Figure 9(c)) were born

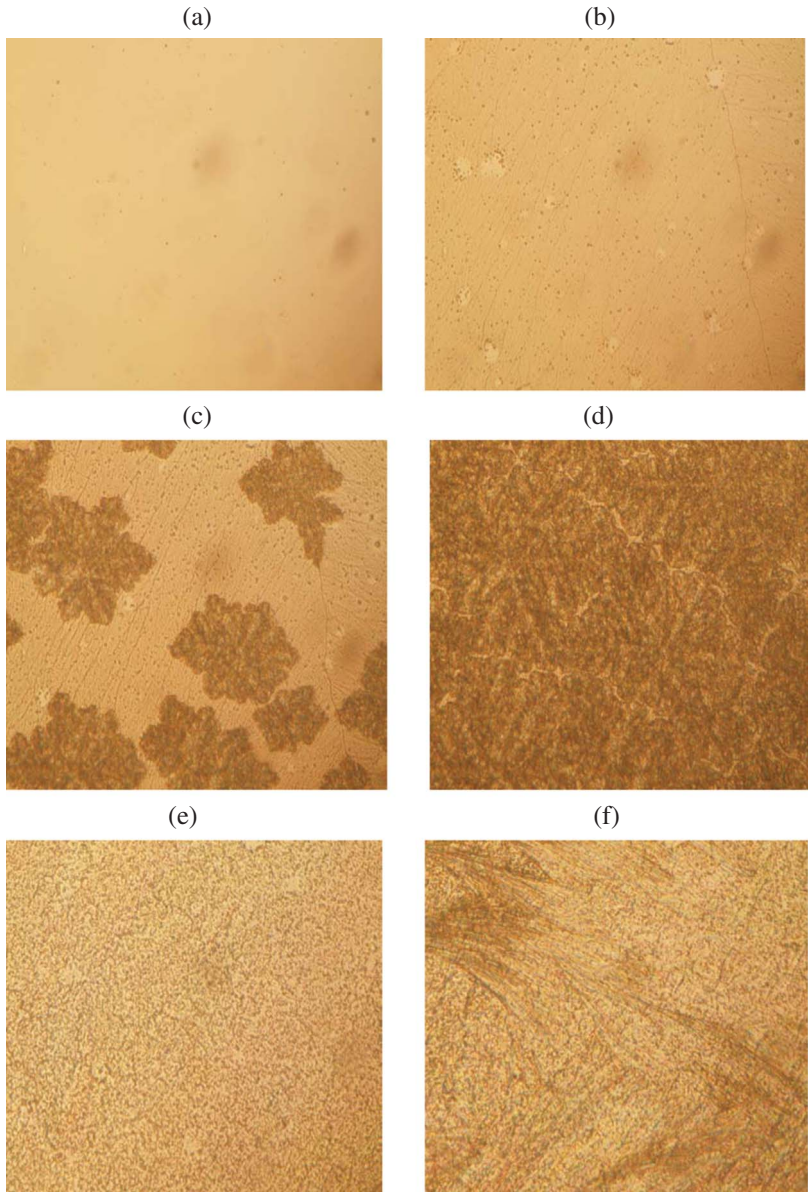

Figure 9. Textures of BABH-16 on cooling at 42 MPa: (a) isotropic liquid at 168°C; (b) the cubic phase at 163°C; (c) the cubic-high-pressure smectic C transition at 155°C; (d) the high-pressure smectic C phase at 154°C; (e) the initial stage of crystallisation at 147°C; (f) the crystalline phase at 140°C (colour version online).

sporadically in the matrix of the Cub phase, and then the SmC(hp) phase (154°C) covered the whole area (Figure 9(d)). On further cooling, the dark thread-like texture suddenly changed to a relatively bright solid (147°C) (Figure 9(e)), and finally changed to the texture of spherulitic crystals (140°C) (Figure 9(f)). Figure 9(e) shows a solid state before the spherulitic crystallisation of BABH-16. It was recognised that the solid state exhibits an initial stage of crystallisation from the SmC(hp) phase. Such a phenomenon often occurred on cooling from the SmC(hp) phase in other BABH-*n* compounds under elevated pressures.

Figure 10 shows the *P*–*T* phase diagrams of BABH-16 constructed on heating and cooling. In the phase diagram on heating, two triple points are observed at 28 MPa and 140°C for the Cr, SmC(hp) and Cub phases, and at 47 MPa and 161°C for the SmC(hp), Cub and I phases, which indicate the lower and upper limits of pressure for the formation of the SmC(hp) and Cub phases, respectively. The SmC(hp)–Cub transition line showed a positive and gentle slope with pressure. Both the phase diagrams are generally similar to those of BABH-14, except for the SmC(hp)–Cub transition line shifting to a higher pressure.

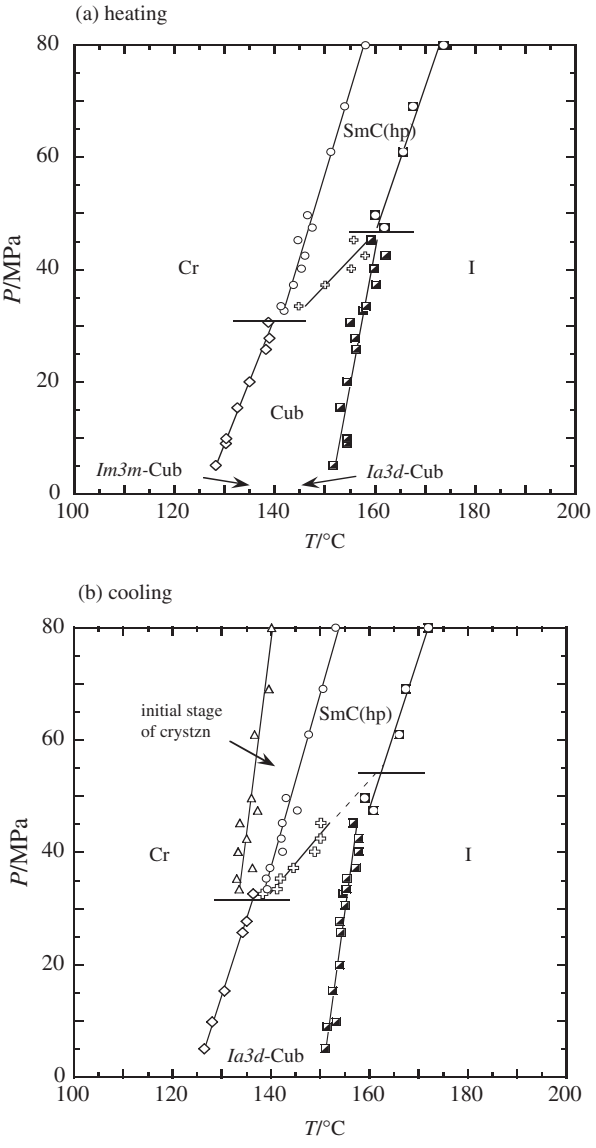

Figure 10. Pressure–temperature phase diagrams of BABH-16 constructed on (a) heating and (b) cooling.

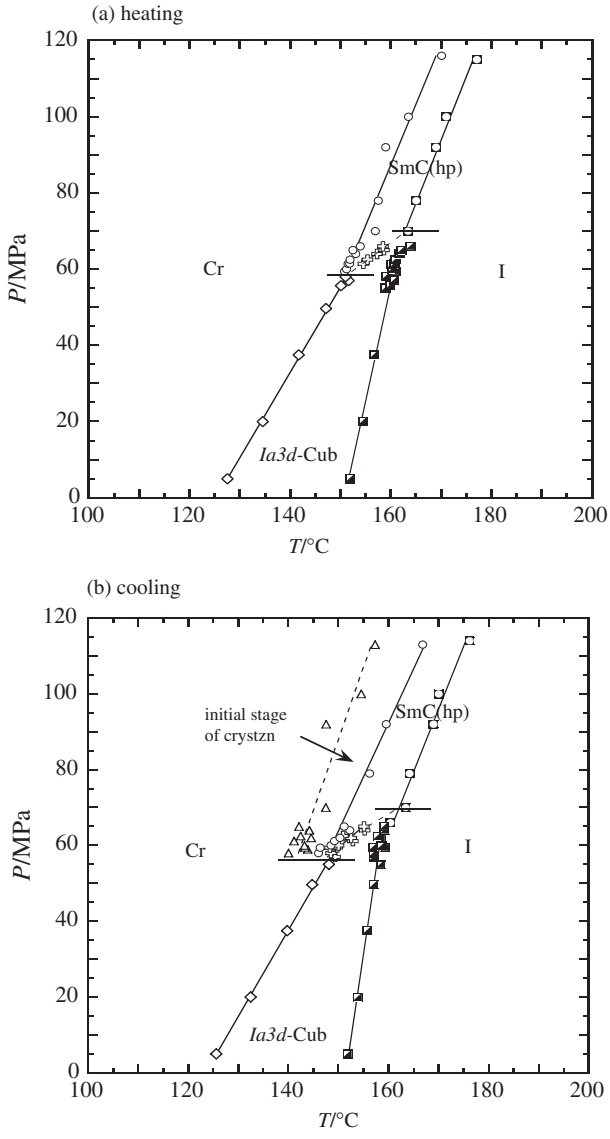

Figure 11. Pressure–temperature phase diagrams of BABH-18 constructed on (a) heating and (b) cooling.

3.5 BABH-18

BABH-18 has the *Ia3d*-type cubic structure and shows the Cr–*Ia3d*-Cub–I phase transition under atmospheric pressure [16]. The phase behaviour of BABH-18 under pressure is generally similar to that of BABH-14 and -16. Figure 11 shows the *P*–*T* phase diagrams of BABH-18 constructed on heating and cooling. The phase behaviour is divided into three pressure regions; the low-pressure region below about 57 MPa, the intermediate-pressure region, and the high-pressure region above about 70 MPa, respectively. The Cr–SmC(hp)–Cub–I phase sequence was recognised in a relatively narrow intermediate-pressure region. The intermediate-pressure region was determined by the SmC(hp)–Cub transition line having a positive and very gentle slope with pressure. There are two triple points. One is 57 MPa and 151°C, at which the Cr, SmC(hp) and Cub phases meet, indicating the lower limit of pressure for the formation of the SmC(hp) phase. The other is 70 MPa and 162°C, at which the SmC(hp), Cub and I phases meet. The solid state region, indicating an initial stage of crystallisation, was observed at temperatures just below the SmC(hp) phase under intermediate- and high-pressures, as shown in Figure 11(b).

3.6 Phase transition sequence of BABH-n

Table 1 lists the phase sequence, the slope of the SmC(hp)–Cub transition, and the triple points for the homologous BABH-*n* compounds ranging from $n = 8$ to $n = 18$. The slope of the Cub–SmC transition changed from negative to positive between BABH-10 and -11, indicating the occurrence of the inversion between the Cub and SmC phases. Then the positive slope of the SmC(hp)–Cub transition decreased from 10 to about 1°C MPa^{-1} with increasing alkoxy chain length from $n = 11$ to $n = 18$. Figure 12 shows the three-dimensional (*P,T,n*) plot of the triple points for the BABH-*n* compounds. The triple point for the Cub phase shows a fold at around $n = 11$, and then increased linearly by 8.85 MPa methylene $unit^{-1}$ with increasing *n* in BABH-11–BABH-18. This exhibits the entropy effect of the longer alkoxy chains at the molecular ends.

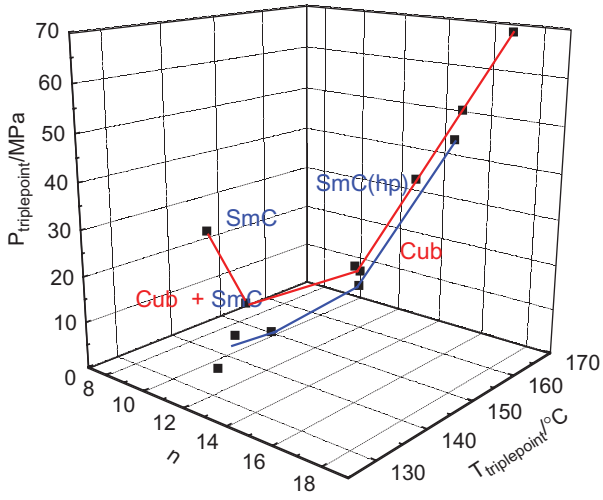

Figure 12. Three-dimensional (P,T,n) plot of the triple points for the homologous BABH-n compounds ranging from n = 8 to n = 18.

4. Discussion

In the BABH-*n* compounds with longer alkyl chains of $n \geq 11$, the SmC(hp) phase appears at the low-temperature side of the Cub phase under intermediate pressures and also exists as a stable mesophase in the high-pressure region. The unusual phase sequence (Cr–*Ia3d*-Cub–SmC–I) for BABH-8 and -10 at atmospheric and low pressures changes to the usual one of Cr–SmC(hp)–Cub–I for BABH-*n* ($n \geq 11$) under intermediate pressures. The experimental results in this study demonstrated that the inversion of the phase sequence between the Cub and SmC phases is induced by applying pressure to the homologous series of BABH-*n* compounds. This phenomenon can be explained well by Saito and Sorai's [22–25] 'alkyl chain as entropy-reservoir' mechanism. One of the authors (S.K.) also explained qualitatively the role of the

Table 1. Phase behaviour of a homologous series of BABH-*n* compounds ranging from $n = 8$ to $n = 18$ under pressure.

	Phase sequence						
			P / MPa				
Pressure region	BABH-8	BABH-10	BABH-11	BABH-12	BABH-14	BABH-16	BABH-18
Low-pressure	*Cr –Cub–SmC–I*				*Cr –Cub–I*		
	0–24	0–10	0–3	0–5	0–15	0–28	0–57
			Cr–Cub ⇄ *I* (*SmC*)				
			3–7				
Intermediate-pressure					*Cr–SmC(hp)–Cub–I*		
			7–10	5–10	15–36	28–47	57–70
High-pressure	*Cr–SmC–I*				*Cr–SmC(hp)–I*		
	>24	>10	>10	>10	>36	>47	>70
Cub–SmC or SmC(hp)–Cub transitions slope (°C/MPa)	–0.5	–1.3	+10.1	+5.8	+1.5	+1.1	+1.0
Triple point							
I *Pt* / MPa			7	5	15	28	57
Tt / °C			138	131	133	140	151
II *Pt* / MPa	24	10	10	10	36	47	70
Tt / °C	144	144	165	160	163	161	162

Note: Triple points I and II indicate the lower and upper limits of pressure for the formation of the SmC(hp) and cubic phases, respectively.

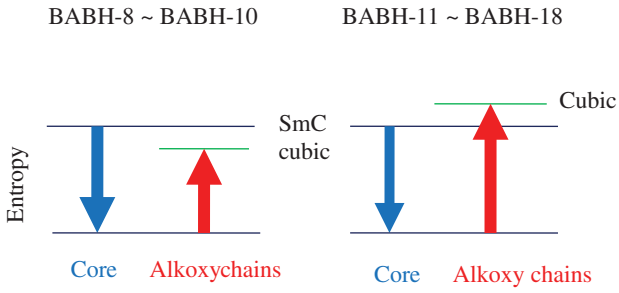

Figure 13. A schematic showing the different contributions of the core and alkoxy chain parts to the entropy of smectic C–cubic transition for BABH-n compounds with shorter and longer alkoxy chains. This is a basic idea for explaining the inversion of phase sequence between the cubic and smectic C phases.

molecular motions of the core and alkyl chains [16]. Based on a thermodynamic analysis of the entropy of transition between the Cub and SmC phases, Saito and Sorai [22–25] addressed the contribution of the two parts to the entropy of transition: one is the aromatic core at the centre and the other is the alkoxy chains at the molecular ends. They contribute oppositely to the entropy of transition. When the effect of the alkoxy chains becomes larger than that of the aromatic core by applying pressure, the phase inversion between the Cub and SmC phases occurs towards the usual SmC→Cub phase sequence. Figure 13 explains the different contributions to the entropy of transition for BABH-*n* compounds with shorter and longer alkoxy chains. This competition accounts for the inversion of the phase sequence in BABH-8 and -10 (Cub→SmC) and BABH-11∼18 (SmC(hp)→Cub). An increase of entropy for the SmC(hp)–Cub transition is due to the radical molecular motion of the longer alkoxy chains at the molecular ends, which contribute to the enrichment of stability for the Cub phase of the BABH-*n*.

The phase behaviour for the *Ia3d* and *Im3m* types of cubic structures is left unresolved in this study, even though it is a very intriguing scientific theme. The X-ray structural analysis of the Cub and SmC(hp) phases for the homologous BABH-*n* compounds under pressure has now been undertaken and will be published in the near future.

Acknowledgements

Shoichi Kutsumizu is grateful for financial support from the Ministry of Education, Culture, Sports, Science, and Technology, Japan [Grant-in-Aid for Scientific Research on Priority Area 'Super-Hierarchical Structures' (No. 446/19022012)] and from the Japan Society for the Promotion of Science [Grant-in Aid for Scientific Research (C) 18550121].

References

[1] Schubert, H.; Hauschild, J.; Demus, D.; Hoffmann, S. *Z. Chem.* **1978**, *18*, 256.
[2] Demus, D.; Gloza, A.; Hartung, H.; Hauser, A.; Rapthel, I.; Wiegeleben, A. *Cryst. Res. Technol.* **1981**, *16*, 1445–1451.
[3] Gray, G.W.; Jones, B.; Marson, F. *J. Chem. Soc.* **1957**, 393–401.
[4] Demus, D.; Kunicke, G.; Neelsen, J.; Sackmann, H. *Z. Naturforsch. A* **1968**, *23*, 84–90.
[5] Gray, G.W.; Goodby, J.W., Eds; *Smectic Liquid Crystals – Textures and Structures*; Leonard Hill: Glasgow, 1984; pp 68–81 (including earlier references on thermotropic cubic mesogens).
[6] Diele, S.; Göring, P. In *Handbook of Liquid Crystals*; Demus, D., Goodby, J., Gray, G.W., Spiess, H.-W., Vill, V., Eds.; Wiley-VCH: Weinheim, 1998; Vol. 2B, pp 887–900.
[7] Bruce, D.W.; Dunmer, D.A.; Hudson, S.A.; Lalinde, E.; Maitlis, P.M.; McDonald, M.P.; Orr, R.; Styling, P. *Mol. Cryst. Liq. Cryst.* **1991**, *206*, 79–92.
[8] Donnio, B.; Heinrich, B.; Gulik-Krywicki, T.; Delacroix, H.; Guillon, D.; Bruce, D.W. *Chem. Mater.* **1997**, *9*, 2951–2965.
[9] Rowe, K.E.; Bruce, D.W. *J. Mater. Chem.* **1998**, *8*, 331–341.
[10] Donnio, B.; Bruce, D.W. *J. Mater. Chem.* **1998**, *8*, 1993–1997.
[11] Luzzati, V.; Spegt, P.A. *Nature (London, UK)* **1967**, *215*, 701–704.
[12] Schoen, A.H. *NASA Technical Note*. No. D-5541; NASA: Washington DC, 1970.
[13] Göring, P.; Diele, S.; Fischer, S.; Wiegeleben, A.; Pelzl, G.; Stegemeyer, H.; Thyen, W. *Liq. Cryst.* **1998**, *25*, 467–474.
[14] Mori, H.; Kutsumizu, S.; Ito, T.; Fukatami, M.; Saito, K.; Sakajiri, K.; Moriya, K. *Chem. Lett.* **2006**, *35*, 362–363.
[15] Kutsumizu, S.; Mori, H.; Fukatami, M.; Saito, K. *J. Appl. Crystallogr*. **2007**, *40*, s279–s282.
[16] Kutsumizu, S.; Mori, H.; Fukatami, M.; Naito, S.; Sakajiri, K.; Saito, K. *Chem. Mater.* **2008**, *20*, 3675–3687.
[17] Maeda, Y.; Saito, K.; Sorai, M. *Liq. Cryst.* **2003**, *30*, 1139–1149.
[18] Maeda, Y.; Ito, T.; Kutsumizu, S. *Liq. Cryst*. **2004**, *31*, 623–632.
[19] Maeda, Y.; Ito, T.; Kutsumizu, S. *Liq. Cryst.* **2004**, *31*, 807–820.
[20] Maeda, Y.; Mori, H.; Kutsumizu, S. *Liq. Cryst.* **2009**, *36*, 217–223.
[21] Maeda, Y.; Koizumi, M. *Rev. Sci. Instrum.* **1996**, *67*, 2030–2031; Maeda, Y.; Koizumi, M. *Rev. High Pressure Sci. Technol.* **1998,** *7*, 1532–1534.
[22] Saito, K.; Sato, A.; Sorai, M. *Liq. Cryst*. **1998**, *25*, 525–530.
[23] Sato, A.; Yamamura, Y.; Saito, K.; Sorai, M. *Liq. Cryst.* **1999**, *26*, 1185–1195.
[24] Saito, K.; Sorai, M. *Chem. Phys. Lett*. **2002**, *366*, 56–61.
[25] Sorai, M.; Saito, K. *Chem. Rec*. **2003**, *3*, 29–39.